

## Article

# Electrochemical Sensor Based on Iron(II) Phthalocyanine and Gold Nanoparticles for Nitrite Detection in Meat Products

Svetlana I. Dorovskikh, Darya D. Klyamer , Anastasiya D. Fedorenko, Natalia B. Morozova and Tamara V. Basova \* 

Nikolaev Institute of Inorganic Chemistry SB RAS, 3 Lavrentiev Pr., 630090 Novosibirsk, Russia; dorov@niic.nsc.ru (S.I.D.); klyamer@niic.nsc.ru (D.D.K.); fedorenko@niic.nsc.ru (A.D.F.); mor@niic.nsc.ru (N.B.M.)  
\* Correspondence: basova@niic.nsc.ru; Tel.: +7-3833309556

**Abstract:** Nitrites are widely used in the food industry, particularly for the preservation of meat products. Controlling the nitrate content in food is an important task to ensure people's health is not at risk; therefore, the search for, and research of, new materials that will modify the electrodes in the electrochemical sensors that detect and control the nitrate content in food products is an urgent task. In this paper, we describe the electrochemical behavior of a glass carbon electrode (GCE), modified with a Fe(II) tetra-tert-butyl phthalocyanine film (FePc(tBu)<sub>4</sub>/GCE), and decorated with gold nanoparticles (Au/FePc(tBu)<sub>4</sub>/GCE); this electrode was deposited using gas-phase methods. The composition and morphology of such electrodes were examined using spectroscopy and electron microscopy methods, whereas the main electrochemical characteristics were determined using cyclic voltammetry (CV) and amperometry (CA) methods in the linear ranges of CV 0.25–2.5 mM, CA 2–120 μM in 0.1 M phosphate buffer (pH = 6.8). The results showed that the modification of bare GCEs, with a Au/FePc(tBu)<sub>4</sub> heterostructure, provided a high surface-to-volume ratio, thus ensuring its high sensitivity to nitrite ions of 0.46 μAμM<sup>-1</sup>. The sensor based on the Au/FePc(tBu)<sub>4</sub>/GCE has a low limit of nitrite detection at 0.35 μM, good repeatability, and stability. The interference study showed that the proposed Au/FePc(tBu)<sub>4</sub>/GCE exhibited a selective response in the presence of interfering anions, and the analytical capability of the sensor was demonstrated by determining nitrite ions in real samples of meat products.

**Keywords:** iron phthalocyanine; gold nanoparticles; nitrite detection; amperometric response



**Citation:** Dorovskikh, S.I.; Klyamer, D.D.; Fedorenko, A.D.; Morozova, N.B.; Basova, T.V. Electrochemical Sensor Based on Iron(II) Phthalocyanine and Gold Nanoparticles for Nitrite Detection in Meat Products. *Sensors* **2022**, *22*, 5780. <https://doi.org/10.3390/s22155780>

Academic Editors: Matteo Mario Scampicchio and Ksenia Morozova

Received: 29 June 2022

Accepted: 29 July 2022

Published: 2 August 2022

**Publisher's Note:** MDPI stays neutral with regard to jurisdictional claims in published maps and institutional affiliations.



**Copyright:** © 2022 by the authors. Licensee MDPI, Basel, Switzerland. This article is an open access article distributed under the terms and conditions of the Creative Commons Attribution (CC BY) license (<https://creativecommons.org/licenses/by/4.0/>).

## 1. Introduction

Sodium nitrite has a number of useful properties, one of which makes this substance indispensable to the food industry. This property provides sausages, and other meat products, with a pink color, which is associated with fresh, high-quality meat. In food products, sodium nitrite is used as a preservative and an antibacterial agent. It prevents the growth of the causative agent of botulism, the metabolic products of which cause severe food poisoning. Nitrites also contribute to the formation of a specific taste and aroma in meat and fish products. At the same time, this dietary supplement is also a poison, an overdose of which may cause severe health consequences. Sodium nitrite is a toxic substance for all mammals; this is because at high concentrations, it binds to hemoglobin in the blood, which causes oxygen starvation in the body as a whole, and in particular, the brain [1]. In addition, when heated (for example, when frying), nitrosamines with carcinogenic properties are formed [2]. The lethal level of nitrites declared by the WHO is in the range of 8.7–28.3 microns [3]; therefore, it is important to develop a fast, cheap, and accurate method for the quantitative determination of nitrite concentrations, especially for controlling the quality of food. In the literature, various early analytical methods were used to determine nitrite concentrations, among them spectrophotometry, chromatography, chemiluminescence, fluorogenic sensing, electrochemical sensing, and so on [4–6].

Of these methods, electrochemical sensors are one of the most effective; this is due to their simple operational technique, rapid response, and lack of interference from nitrate ions and other interfering analytes [7]. Electrochemical methods based on the detection of ions formed during the reduction of nitrites are not used in practice, because they suffer from poor sensitivity and are subject to several interferences [8]. The electrochemical oxidation of nitrite ions is preferable, and is based on the direct reaction of its oxidation to nitrate [9]. It should be noted that nitrite oxidation is associated with a relatively higher overpotential when using a bare glass carbon electrode; therefore, the search for, and study of, materials that will modify electrodes that contribute to decreasing overpotential during nitrite oxidation is an urgent task. In addition, the modification of electrode surfaces may provide a way to extend the dynamic range in analytical determinations.

To determine nitrites, various materials are used to modify the surface of electrodes. Among them are conductive polymers, such as PEDOT and polyaniline, in addition to their composites, which have electroactive molecules and metal nanoparticles (MNPs); for example, PEDOT/PAS (PAS is a polyacenic semiconductor) [10], polyaniline/MoS<sub>2</sub> [11], nano-sized hydroxyapatite/PEDOT [12], and AuNC/PEDOT [13]. Nanocarbon materials and their composites are also widely used in the modification of the electrodes in the electrochemical sensors that detect nitrite ions; for example, rGO/MWCNTs [14], rGO/ferrocene [15], PtNPs loaded Ni(OH)<sub>2</sub>/multi-walled carbon nanotube composites [16], chitosan/Prussian blue nanoparticles in a mixture of graphene nanosheets and carbon nanospheres [17], and many others.

Metal phthalocyanines (MPc) and porphyrins, especially Co(II)Pc and Fe(II)Pc derivatives, are also used for the electrochemical detection of nitrites [18–22] due to their remarkable physicochemical and electronic properties, as well as their excellent catalytic activity and electron mediator capabilities in various electrochemical reactions [23–25]. Catalytic activity is mainly observed in phthalocyanine complexes containing electrochemically active metals such as Cu, Co, Fe, and Mn. To modify electrodes, phthalocyanines are usually deposited by spin coating, drop casting [7,20,26], electropolymerization [27], layer-by-layer deposition [28], and through use of the covalent modification approach [29]. Films of unsubstituted MPcs and their fluoro-, chloro-, and tert-butyl substituted derivatives can also be prepared using physical vapor deposition [30,31]; however, attempts to apply them to the modification of electrodes in electrochemical sensors have not been so fruitful.

Noble metal nanoparticles (MNP) by themselves, and in combination with other materials, have also been utilized in a number of electrochemical applications, such as electrocatalysis, electrochemical analysis, and electrochemical sensing. They are used because of their catalytic properties, which usually occur due to chemisorption on the surface. Another important feature of metal nanoparticles is their high surface area to volume ratio, which is important for sensor applications. A synergetic combination of the properties of phthalocyanines and metal nanoparticles is known to result in the improvement of the sensor properties of MNP/MPc hybrid materials [32], including their sensor response to nitrites [33–36]. Facilitating mediated electron transfer through the use of AuNPs, in combination with phthalocyanine, may also be important in the creation of cellular biosensors [37–39]. In most studies, gold nanoparticles were obtained using “wet” methods or electrodeposition. Gas-phase methods, such as physical vapor deposition and chemical vapor deposition, are used less frequently in the modification of electrodes with gold nanoparticles, although they allow nanoparticles to be obtained with a metal content close to 100%, without any surfactants or stabilizers [40].

In this paper, we describe the electrochemical behavior of a glass carbon electrode (GCE) modified with a Fe(II) tetra-tert-butyl phthalocyanine film (FePc(tBu)<sub>4</sub>/GCE), decorated with gold nanoparticles (Au/FePc(tBu)<sub>4</sub>/GCE), which was deposited using gas-phase methods. The composition and morphology of such electrodes were examined using spectroscopy and electron microscopy methods, whereas the main electrochemical characteristics were determined using cyclic voltammetry (CV) and amperometry (CA) methods in 0.1 M phosphate buffer (pH = 6.8). Results showed that the modification of the

FePc(tBu)<sub>4</sub>/GCE, using gold nanoparticles, caused the sensor to become more sensitive nitrite ions, and the detection limit substantially decreased. The interference study showed that the proposed Au/FePc(tBu)<sub>4</sub>/GCE exhibited a selective response in the presence of interfering anions, and the analytical capability of the sensor was demonstrated by determining nitrite ions in real samples of meat products. All components of the proposed sensors are comparatively cheap and commercially available. Moreover, they were deposited on the surface of GCE using a physical vapor deposition technique, which makes it possible to control the ratio of components in the heterostructure and to obtain a large number of electrodes in one deposition cycle.

## 2. Materials and Methods

### 2.1. Materials

FePc(tBu)<sub>4</sub> was prepared by heating a mixture of 4-tert-butylphthalonitrile (Sigma-Aldrich, St. Louis, MI, USA, CAS 32703-80-3) and iron(II) chloride (Sigma-Aldrich, Saint Louis, USA, CAS 7758-94-3) at 220 °C, which was purified by sublimation in a vacuum (10<sup>-5</sup> Torr). The metallic gold—Au (99.99%)—was provided by the Novosibirsk Refining Company, Ltd., Russia. The sodium nitrite—NaNO<sub>2</sub> (>99%)—was obtained from Reactive Ltd., Moscow, Russia. The phosphate buffer solution (PBS, 0.1 M), with a pH value of 6.8, was provided by VWR Chemicals LLC, Wayne, PA, USA. The hexaammineruthenium(II) chloride—Ru(NH<sub>3</sub>)<sub>6</sub>Cl<sub>2</sub> (>99.9%, CAS No. 15305-72-3)—was provided by Sigma Aldrich, Saint Louis, USA. The glassy carbon electrodes—GCE (SIGRADUR<sup>®</sup> G GGE plates 10 × 10 mm<sup>2</sup>, d = 1 mm)—were provided by Chemservice Ltd., Moscow, Russia. Other reagents (NaCl, NaNO<sub>3</sub>, glucose, sodium glutamate, sodium ascorbate, buffer electrolytes with pH values of 1.7 (phthalate buffer), 3.6 (acetic buffer), 5.6 (ammonium acetate 0.2 M—Sodium citrate tribasic buffer), 7.4 (PBS buffer), 9.2 (sodium tetraborate)) were of analytical grade (Dia-m Ltd., Novosibirsk, Russia) and used as received without further purification.

### 2.2. Electrodes Preparation

Initially, the GCE plates were washed with sulfuric acid and nitric acid, then degreased with sodium hydroxide and ethanol, and finally dried at room temperature. Layers of FePc(tBu)<sub>4</sub> were deposited by a PVD method on the surface of GCE plates (samples FePc(tBu)<sub>4</sub>/GCE). The deposition conditions were as follows: the total pressure was 5 × 10<sup>-5</sup> Torr, the evaporation temperature was 450 °C, the deposition time was 1 h, and the substrate temperature was 60 °C. The samples of the Au/FePc(tBu)<sub>4</sub>/GCEs were prepared using PVD of gold onto FePc(tBu)<sub>4</sub>/GCE at P = 10<sup>-6</sup> Torr. The deposition conditions were as follows: the gold load was 6 mg, the evaporator temperature was 1532 °C, and the substrate temperature was 100 °C.

### 2.3. Instrumentation

The gold content in the Au/FePc(tBu)<sub>4</sub>/GCE sample was determined using inductively coupled plasma atomic emission spectroscopy (ICP-AES), using a high-resolution spectrometer iCAP 6500 Duo (Thermo Fisher Scientific, Waltham, MA, USA). The HCl (ACS reagent, 37%), HNO<sub>3</sub> (70%, purified by redistillation—99.999% trace metals basis), deionized water (purified with the Direct-Q3 system (Millipore, Burlington, MA, USA) >18 MU/cm), Ar gas (99.999%), and the Gold Standard for ICP TraceCERT<sup>®</sup>, 1000 mg/L Au in hydrochloric acid, were used as reagents to determine the gold content. The sample was washed off with a minimum amount of concentrated HCl and HNO<sub>3</sub> (3:1), and the solution was injected into plasma using a SeaSpray type nebulizer with a peristaltic pump. The working parameters of the ICP-AES system are as follows: power supply—1150 W; nebulizer argon flow rate—0.70 L min<sup>-1</sup>; auxiliary—0.50 L min<sup>-1</sup>; and cooling—12 L min<sup>-1</sup>. The data acquisition and processing were carried out with the iTEVA (Thermo Scientific, Philadelphia, PA, USA) software.

The chemical state of GCE, FePc(tBu)<sub>4</sub>/GCE, and Au/FePc(tBu)<sub>4</sub>/GCE was investigated using X-ray photoelectron spectroscopy (XPS). The XPS measurements were performed

using the FlexPS system (Specs GmbH, Berlin, Germany) with a PHOIBOS 150 analyzer and monochromatic Al K $\alpha$  radiation at 1486.71 eV. The XPS spectra were fitted using a Gaussian–Lorentzian convolution function after a Shirley background subtraction. The binding energies were calibrated to the C 1s peak for C–C group at 284.6 eV.

The surface morphology of the GCE, FePc(tBu)<sub>4</sub>/GCE, and Au/FePc(tBu)<sub>4</sub>/GCE was investigated using a scanning electron microscope (JEOL–JSM 6700 F, Tokyo, Japan) and atomic force microscope (Solver Pro, Moscow, Russia).

The cyclic voltammetry (CV) and amperometry measurements were carried out using a potentiostat–galvanostat (P8-S, Electrochemical Instruments Ltd., Moscow, Russia) to evaluate the electrochemical activity of the studied electrodes in relation to the NO<sub>2</sub><sup>−</sup> ions, and to determine their sensory characteristics in relation to NO<sub>2</sub><sup>−</sup>. The electrochemical cell E-7SF (Electrochemical Instruments Ltd., Moscow, Russia) was assembled using a conventional three-electrode system: a saturated Ag/AgCl reference electrode, a Pt wire auxiliary electrode, and the prepared working electrodes (GCE, FePc(tBu)<sub>4</sub>/GCE, or Au/FePc(tBu)<sub>4</sub>/GCE). All potentials referred to this reference electrode.

CV curves of the GCE and FePc(tBu)<sub>4</sub>/GCE were recorded in the range of potentials from −300 to 1200 mV. In the case of the Au/FePc(tBu)<sub>4</sub>/GCE, along with peaks of nitrite ion oxidation, gold oxidation peaks (at 1060 mV) were also recorded in this region (Figure S1, Supporting Information (SI)). Since the process of gold oxidation at potentials above 1060 mV proceeds irreversibly, the CV curves of the Au/FePc(tBu)<sub>4</sub>/GCE were recorded in the potential range of −300–1000 mV in order to avoid degradation of the samples. The concentration of NO<sub>2</sub><sup>−</sup> varied from 0.25 to 2.5 mM. The sweep rates ( $v$ ) ranged from 100 to 500 mV/s.

The CV curves of the FePc(tBu)<sub>4</sub>/GCE and Au/FePc(tBu)<sub>4</sub>/GCE samples were recorded at a nitrite concentration of 1.25 mM, and at a scanning rate of 100 mV/s, with a change in the pH of the electrolyte in the range of 1.7 to 9.2.

The active surface areas of the GCE, FePc(tBu)<sub>4</sub>/GCE, and Au/FePc(tBu)<sub>4</sub>/GCE were determined using a Ru<sup>2+</sup>/Ru<sup>3+</sup> redox system, in accordance with the Randles–Sevcik Equation (1) for reversible systems [36]:

$$I_{pa} = 2.69 \times 10^5 n^3/2 ACD^{1/2} v^{1/2}, \quad (1)$$

where  $D$  and  $C$  are the diffusion coefficient ( $7.7 \times 10^{-6}$  cm<sup>2</sup>/s [41]) and concentration of the redox probe ( $2 \times 10^{-6}$  mol/cm<sup>3</sup> [Ru(NH<sub>3</sub>)<sub>6</sub>]Cl<sub>2</sub>), respectively;  $n$  is the number of electrons transferred ( $n = 1$ ),  $v$  is the scan rate (0.001 V/s), and  $A$  is the active surface area of the electrode.

The surface coverage of the electroactive sites of the modified GCE samples was determined from the corresponding CV curves (See Section 3.2) using Equation (2) [36]:

$$\Gamma = Q/nFA, \quad (2)$$

where  $\Gamma$  is the surface coverage,  $Q$  is determined by integrating the area under the anodic peak,  $n$  is the number of transferred electrons ( $n = 1$ ),  $F$  is the Faraday constant, and  $A$  is the active surface area of the electrode.

The amperometric studies of FePc(tBu)<sub>4</sub>/GCE and Au/FePc(tBu)<sub>4</sub>/GCE were performed at  $E = 1$  V in an Ar (99.999%, Company “Chisty Gasy”, Novosibirsk, Russia) atmosphere. To test the selectivity of the Au/FePc(tBu)<sub>4</sub>/GCE, NaCl, NaNO<sub>3</sub>, glucose, sodium glutamate, and sodium ascorbate (Na(AA)) were used as interfering compounds. The amperometric measurements were carried out in 0.1 M PBS (pH 6.8) at 1.0 V vs. Ag/AgCl. The concentration of each interfering compound (except Na(AA)) was 50  $\mu$ M, which is 25 times higher than the concentration of NO<sub>2</sub><sup>−</sup> (2  $\mu$ M). The concentration of Na(AA) was 20  $\mu$ M, taking into account the data concerning the standard Na(AA)/NaNO<sub>2</sub> ratios in real meat products, as described in the literature [42,43]. The stability of the response of the Au/FePc(tBu)<sub>4</sub>/GCE to nitrite was studied using amperometric measurements at 24,

48, and 168 h. The reproducibility of the Au/FePc(tBu)<sub>4</sub>/GCE was investigated by CV, measuring five independently prepared identical sensors.

#### 2.4. Preparation of Meat Food Samples

Samples of meat products (smoke sausage, sausage produced by the Siberian Food Company Ltd., Novosibirsk, Russia) were purchased at a local supermarket (Supermarket "Yarche", Novosibirsk, Russia). To study the electrochemical characteristics, the food samples were pretreated, in accordance with a method described elsewhere [7,18]. In brief, preparation of the supernatant solution involved the following steps: 5.0 g of the food samples were cut into small pieces and mixed with 20 mL of distilled water. The mixture was transferred into a grinder, and it was squeezed until the mixture was crushed. This was followed by ultrasonication for 30 min. After the ultrasonic treatment, the supernatant solution was filtered and heated at 70 °C for 40 min to remove traces of proteins and to make the supernatant solutions homogeneous. Finally, the supernatant solution was diluted in 100 mL of 0.1 M PBS solution (pH 6.8) for further electrochemical analysis of nitrites. To prevent the degradation of nitrites, the supernatant solution was stored at −10 °C.

#### 2.5. Statistical Analysis

Based on the recommendations given in [6], the main validation parameters (precision, repeatability, and trueness) for the nitrite determination method, using the amperometric calibration curve for Au/FePc(tBu)<sub>4</sub>/GCE (See Section 3.8), were assessed. A standard addition method was used for calibration in the laboratory.

The accuracy parameter was assessed by calculating the relative standard deviation (RSD) for five parallel determinations, using standard solutions, with a certain concentration of nitrite. To assess repeatability, the analysis of three replicates of 5 μM standard solutions was performed on the same day; a week later, it gave a 5% RSD value.

The trueness was determined through the recovery evaluation. Five parallel detections, using standard solutions with a certain concentration of nitrite, were carried out in order to determine the recovery of the proposed calibration; this was defined in terms of the ratio of found NO<sub>2</sub><sup>−</sup> concentrations to the added concentration: %R = 100(C<sub>found</sub>)/C<sub>added</sub>.

### 3. Results and Discussion

#### 3.1. Characterization of the FePc(tBu)<sub>4</sub>/GCE and Au/FePc(tBu)<sub>4</sub>/GCE

The surface of a bare GCE is porous, and it is formed by oval agglomerates with dimensions of 80–200 nm (Figure 1a,b). The EDS data are given in Figure S2 (SI). The average roughness of the bare GCE is 112 nm (scan area 10 × 10 μm<sup>2</sup>). The FePc(tBu)<sub>4</sub> film repeats the topography of the bare GCE. According to XRD analysis, the FePc(tBu)<sub>4</sub> film is amorphous. In the XPS spectrum of the FePc(tBu)<sub>4</sub>/GCE sample, the characteristic C 1s, N 1s, and Fe 2p lines, which are related to the FePc(tBu)<sub>4</sub> films, were observed (Figure 1c). The Fe 2p spectra consist of two peaks: one asymmetric peak at around 711 eV, which come from the electrons at the Fe 2p<sub>3/2</sub> level, and another, less intense peak at approximately 724 eV, which come from Fe 2p<sub>1/2</sub> electrons. The fitting components at 709.9 and 723.1 eV are assigned to Fe<sup>2+</sup> [44]. The low intense lines at 712.3 and 725.2 eV may be due to a decrease in electron density around the Fe atom; this is because of the delocalization of the π-electron system during the adsorption of FePc(tBu)<sub>4</sub> on the GCE matrix [45].

An estimation of the carbon concentration, in relation to the iron phthalocyanine, shows that the C 1s spectrum is mainly determined by the FePc(tBu)<sub>4</sub> structure. Since FePc(tBu)<sub>4</sub> has an extended π-system, it is characterized by the presence of 'shake-up' satellites in the C 1s and N 1s spectra [46–49]. Thus, all of the observed C 1s peaks (Figure 1d) at 284.6 eV (C-C), 285.8 eV (C-N), 287.3 eV, and 288.4 eV can be attributed to the FePc(tBu)<sub>4</sub> film. The second peak, observed at about 285.8 eV, comes from the eight pyrrole carbon atoms of FePc(tBu)<sub>4</sub>. The low intense C 1s peak, observed at about 287.3 eV and 288.4 eV, is associated with the benzene and pyrrole carbon shake-up transitions of FePc(tBu)<sub>4</sub> [47–49]; however, the regions of the C 1s peaks, at approximately 284.6 eV, 287.3 eV, and 288.4 eV,

are associated with the carbon atoms in the phthalocyanine rings. Moreover, small contributions can be produced by the aromatic carbon, C=O, and COOH groups in the GCE, respectively. In the N 1s spectra of the FePc(tBu)<sub>4</sub>/GCE (Figure S3, Supporting Information), the line at 398.8 eV can be associated with two nonequivalent nitrogen types that cannot be distinguished in the spectrum due to their almost identical binding energies, whereas the low-intensity line at 400.3 eV can be attributed to a satellite structure, which is a ‘shake-up’ of four pyrrolic nitrogens Fe-N [46–48]. The O 1s spectra (Figure S3) show two components that are related to a carbon-bound oxygen (531.8 eV) and a small amount of adsorbed water or a OH group (533.5 eV). Quantitative analysis shows that the N: Fe concentration ratio is close to eight, which is within the XPS margin of error.

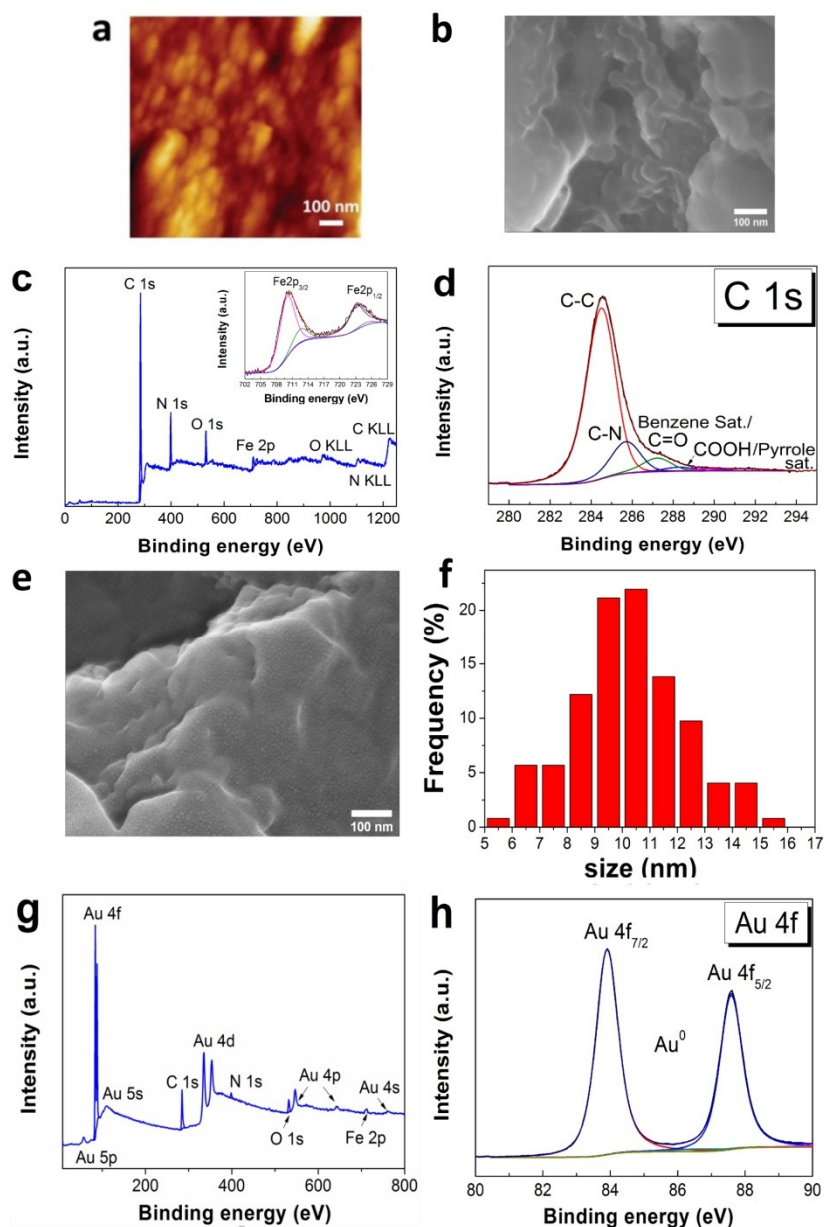


**Figure 1.** AFM image of a bare GCE (a); SEM image of the FePc(tBu)<sub>4</sub>/GCE (b); XPS spectrum of the FePc(tBu)<sub>4</sub>/GCE with Fe 2p (c); fitting of the C 1s spectra (d); SEM image of the Au/FePc(tBu)<sub>4</sub>/GCE (e) with AuNPs size distribution (f); XPS spectrum of the Au/FePc(tBu)<sub>4</sub>/GCE (g); and fitting of the Au 4f spectra (h).

After the gold deposition, uniformly distributed AuNPs are visualized on the surface of the Au/FePc(tBu)<sub>4</sub>/GCE sample (Figure 1e). The average sizes of AuNPs in Au/FePc(tBu)<sub>4</sub>/GCE

are 9–11 nm (Figure 1f). Along with Au 4f lines, the low-intensity Fe 2p, C 1s, and N 1s lines, which are related to FePc(tBu)<sub>4</sub>, are observed on the XPS spectrum of the Au/FePc(tBu)<sub>4</sub>/GCE (Figure 1g), thus confirming the formation of the Au/FePc(tBu)<sub>4</sub> heterostructure on the GCE surface. The positions of the main Au 4f peaks indicate the presence of metallic gold (Au 4f<sub>7/2</sub> 84.1 eV) (Figure 1h). From the EDS data (Figure S2), the composition of the Au/FePc(tBu)<sub>4</sub>/GCE (at.%) is C: 54.1; Au: 21.3; N: 16.1; O: 5.6; Fe: 2.3; and Si: 0.6. The average gold content in the Au/FePc(tBu)<sub>4</sub>/GCE, determined using ICP-AES, is  $4.7 \pm 0.5 \mu\text{g}/\text{cm}^2$ .

### 3.2. Charge Transfer Behavior of GCE, FePc(tBu)<sub>4</sub>/GCE and Au/FePc(tBu)<sub>4</sub>/GCE

The charge transfer behavior of the GCE, FePc(tBu)<sub>4</sub>/GCE, and Au/FePc(tBu)<sub>4</sub>/GCE samples were studied using CV measurements in a solution containing 2 mM [Ru(NH<sub>3</sub>)<sub>6</sub>]Cl<sub>2</sub> (Figure 2). Hexaammineruthenium (II)/(III) is a universal and convenient couple that is used to study the electron transfer behavior of an electrode, as well as to estimate the electrode surface area [50,51]. Recent works emphasized the advantages of using this couple due to its stability during electron transfers, and the absence of the co-called ‘aerial oxidation’ effect [52]. This couple is also used to study the electrochemical properties of gold-containing electrodes [53,54].

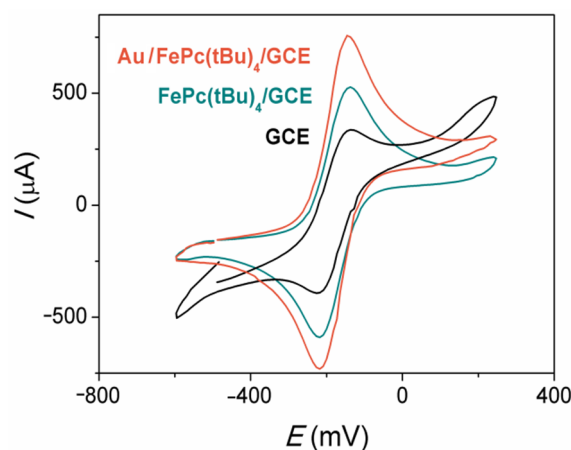


**Figure 2.** CV curves of the bare GCE, FePc(tBu)<sub>4</sub>/GCE, and Au/FePc(tBu)<sub>4</sub>/GCE in 2 mM [Ru(NH<sub>3</sub>)<sub>6</sub>]Cl<sub>2</sub> in 0.5 M KCl. Scan rate is 9.9 mV/s.

The bare GCE demonstrates a reversible behavior during the single electron transfer of the Ru<sup>2+</sup>/Ru<sup>3+</sup> redox reaction, with a peak-to-peak separation ( $\Delta E_p$ ) value of 84 mV (Table 1, column 2). The modification of a GCE surface with FePc(tBu)<sub>4</sub> film or a Au/FePc(tBu)<sub>4</sub> heterostructure leads to a decrease in the values of  $\Delta E_p$ . Both the FePc(tBu)<sub>4</sub>/GCE and Au/FePc(tBu)<sub>4</sub>/GCEs exhibit a reversible behavior in the Ru<sup>2+</sup>/Ru<sup>3+</sup> redox reaction. A comparison of the current ( $I_{pa}$ ) values of the Ru<sup>2+</sup>/Ru<sup>3+</sup> peak (Table 1, column 3) in the series of GCE, FePc(tBu)<sub>4</sub>/GCE, and Au/FePc(tBu)<sub>4</sub>/GCE samples indicates that the best electron transfer behavior is exhibited in the Au/FePc(tBu)<sub>4</sub>/GCE. It is assumed that the presence of AuNPs provides a high surface-to-volume ratio, thus contributing to good electron transfers between the redox probe and the Au/FePc(tBu)<sub>4</sub>/GCE.

**Table 1.**  $\Delta E_p$ ,  $I_{pa}$ , and A values of the GCE, FePc(tBu)<sub>4</sub>/GCE, and Au/FePc(tBu)<sub>4</sub>/GCE samples.

Electrode <sup>1</sup>	$\Delta E_p$ (mV)	$I_{pa}$ ( $\mu\text{A}$ )	A ( $\text{cm}^2$ )
GCE	84	681	0.413
FePc(tBu) <sub>4</sub> /GCE	80	744	0.451
Au/FePc(tBu) <sub>4</sub> /GCE	76	863	0.523

<sup>1</sup> Geometrical surface area of the electrode is 0.283 cm<sup>2</sup>.

The average active surface area values of the GCE, FePc(tBu)<sub>4</sub>/GCE, and Au/FePc(tBu)<sub>4</sub>/GCE were calculated from three identical samples of each type, and they are given in Table 1. Their average roughness factors (the ratios of *A* values to geometrical surface area) are 1.46, 1.59, and 1.84, respectively. The  $\Gamma$  values were found to be  $0.9 \times 10^{-9}$  and  $2.2 \times 10^{-9}$  mol·cm<sup>-2</sup> for the FePc(tBu)<sub>4</sub>/GCE and Au/FePc(tBu)<sub>4</sub>/GCE, respectively. These values are comparable to, or even higher than, those of other electrodes that are modified with metal phthalocyanines [55] or AuNPs [35,56].

Thus, the modification of a bare GCE with FePc(tBu)<sub>4</sub> film or a Au/FePc(tBu)<sub>4</sub> heterostructure provides a high surface-to-volume ratio, which therefore makes these samples promising for further use as electrochemical sensors.

### 3.3. Effect of the Electrolyte pH on Nitrite Oxidation

The effect of electrolyte pH on the potentials and current values of nitrite oxidation, as it occurs on the FePc(tBu)<sub>4</sub>/GCE and Au/FePc(tBu)<sub>4</sub>/GCE, was studied in order to select the optimal conditions for further investigation of the nitrite oxidation response. FePc(tBu)<sub>4</sub> demonstrates a reversible behavior during single-electron transfer, in a pH range of 1.7 to 7.4 (Figure 3a). The positions of both of the redox peaks Fe<sup>2+</sup>/Fe<sup>3+</sup> and the nitrite oxidation peaks shifted towards positive potentials with increasing proton concentrations. It is possible that an excess of anions (pH < 3.5) and hydroxy groups (pH > 7.5) blocked the active centers of the electrode, thus hindering electron transfer [57]. The same trend was almost observed on the FePc(tBu)<sub>4</sub>/GCE.

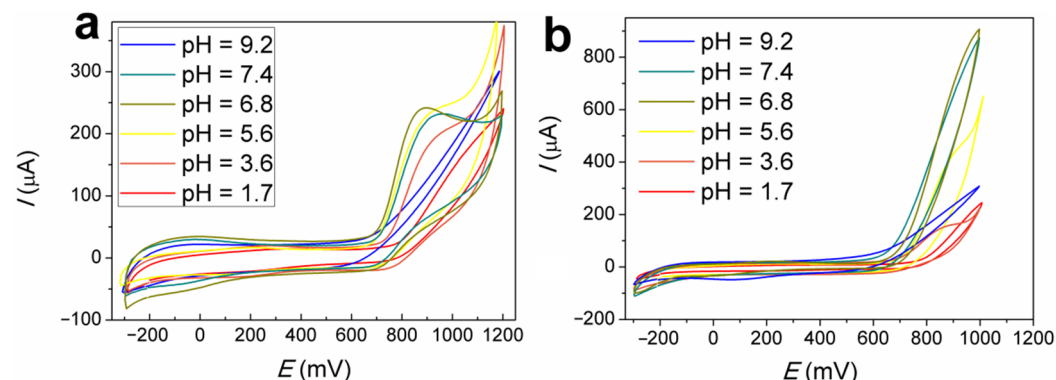


**Figure 3.** CVs curves of the FePc(tBu)<sub>4</sub>/GCE (a) and Au/FePc(tBu)<sub>4</sub>/GCE (b), recorded in electrolytes with various pH balances, containing 1.25 mM NaNO<sub>2</sub>, at a scanning rate of 100 mV/s.

Nitrite ions are known to have a low stability in acidic media [58], and the efficiency of the nitrite ion oxidation process decreases with an increase in pH > 7.5 [34,59]. Consequently, the highest current values of nitrite oxidation for both electrodes are in the pH range of 5.6–7.4. The maximal nitrite oxidation current, together with the lowest oxidation potential (905 mV), is achieved at a pH value close to six; this caused greatest level of activity on FePc(tBu)<sub>4</sub>/GCE. After decorating the FePc(tBu)<sub>4</sub>/GCE with AuNPs, its proclivity for nitrite oxidation increases, and the current nitrite oxidation on this electrode reaches a maximum of pH = 7; therefore, the electrolyte with a pH = 6.8 is optimal for studying the electrochemical behavior of both the FePc(tBu)<sub>4</sub>/GCE and Au/FePc(tBu)<sub>4</sub>/GCE with regard to nitrite oxidation.

### 3.4. Cyclic Voltammetry Characterization of GCE, FePc(tBu)<sub>4</sub>/GCE, and Au/FePc(tBu)<sub>4</sub>/GCE

From the CV curves of the GCE (Figure 4a), FePc(tBu)<sub>4</sub>/GCE (Figure 4c), and Au/FePc(tBu)<sub>4</sub>/GCE (Figure 4e), at a recorded pH = 6.8, in the range of nitrite concentrations from 0.25 to 2.5 mM, the peaks associated with the oxidation of nitrate ions (anodic branch) were detected at 1020, 905, and 875 mV, respectively.

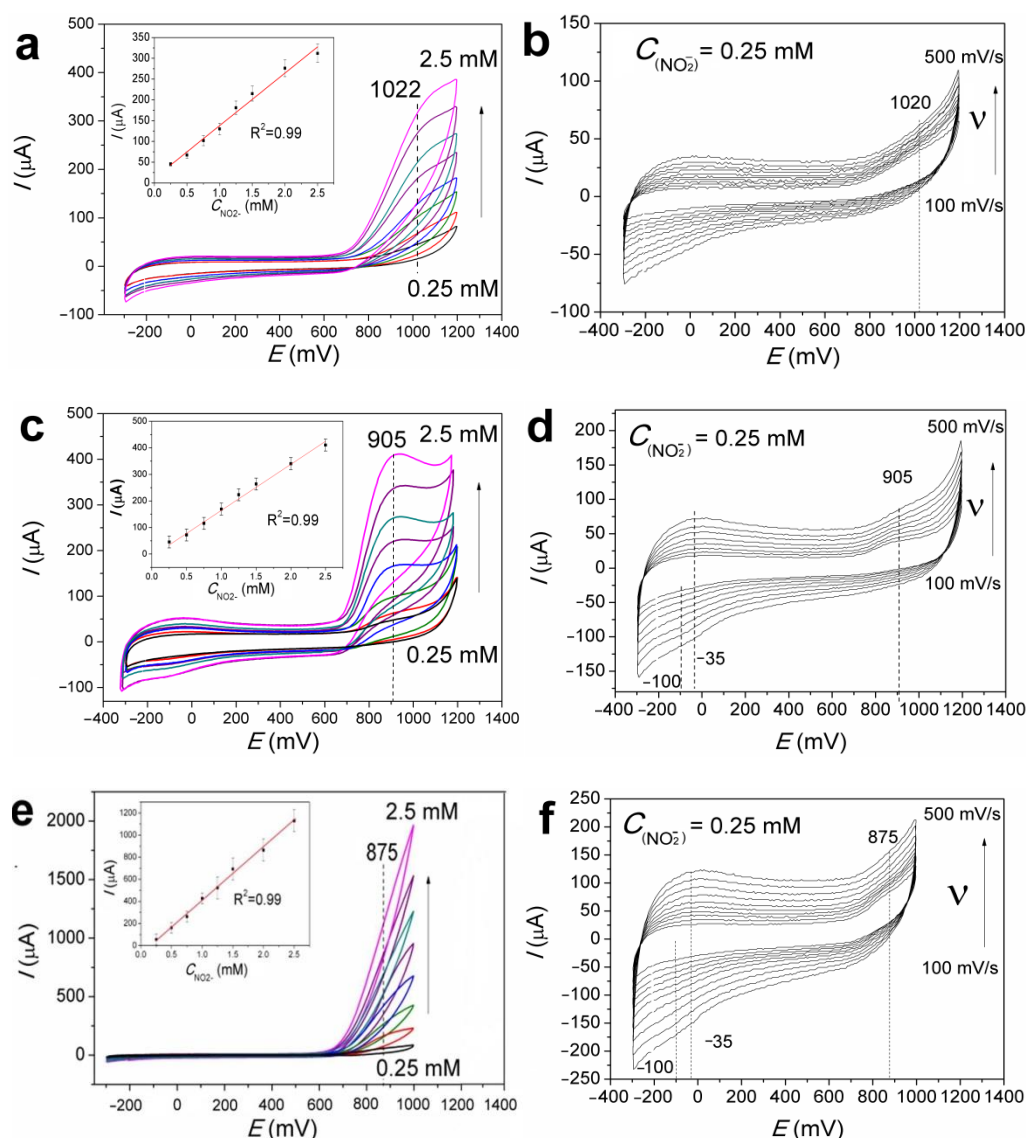


**Figure 4.** CV curves of the bare GCE, FePc(tBu)<sub>4</sub>/GCE, and Au/FePc(tBu)<sub>4</sub>/GCE in the nitrite concentration range of 0.25 to 2.5 mM (a,c,e) and at different scan rates from 100 to 500 mV/s (b,d,f).

The peaks related to the redox processes of FePc(tBu)<sub>4</sub> are observed at  $-100$  and  $-35$  mV, as in the cases of the FePc(tBu)<sub>4</sub>/GCE and Au/FePc(tBu)<sub>4</sub>/GCE (Figure 4). An increase in the peak current of nitrite oxidation ( $I$ ), on the CV curves of the studied samples, with an increase in the concentration of  $\text{NO}_2^-$ , indicates a high sensitivity to the studied electrodes; this is especially true of the Au/FePc(tBu)<sub>4</sub>/GCE in the oxidation reaction with nitrite ions. It should be noted that in the studied series of samples, peaks related to the nitrate ion reduction process are absent on the CV curves. This indicates that the nitrite irreversibly oxidizes on the surfaces of these electrodes. The shift of the peaks during the oxidation of nitrite ions from 1020 to 875 mV indicates that the modification of the GCE surface facilitates the electrochemical oxidation process on the surfaces of the FePc(tBu)<sub>4</sub>/GCE and Au/FePc(tBu)<sub>4</sub>/GCE.

According to the data in the literature, peaks corresponding to nitrite oxidation lie in the range of 0.8–1 V (PBS, pH = 5.8–7) in the case of electrodes that are modified with transition metal phthalocyanines [21,24,33,34,59], and in the range of 0.6–0.9 V in the case of electrodes that are modified with AuNPs (PBS, pH = 5–8) [34–36,60]. The potential values of the FePc(tBu)<sub>4</sub>/GCE and Au/FePc(tBu)<sub>4</sub>/GCE studied in this work correspond well

with the data in the literature, which also indicates their possible use in sensors which determine the presence of nitrites.

### 3.5. The Mechanism of Nitrite Oxidation on the FePc(tBu)<sub>4</sub>/GCE and Au/FePc(tBu)<sub>4</sub>/GCE

To gain insight into the mechanism of nitrite oxidation, which occurred on both the FePc(tBu)<sub>4</sub>/GCE and Au/FePc(tBu)<sub>4</sub>/GCE, CV curves at different  $\nu$  (100–500 mV/s) in 0.25 mM nitrite were recorded (Figure 4b,d,f). For both the FePc(tBu)<sub>4</sub>/GCE and Au/FePc(tBu)<sub>4</sub>/GCE, linear dependencies between the current peaks of nitrite oxidation and the square of the scan rates are shown in Figure 5a,c, and the corresponding dependencies are given in Table 2. The linearity of these dependencies may indicate that the process of nitrite oxidation on the FePc(tBu)<sub>4</sub>/GCE and Au/FePc(tBu)<sub>4</sub>/GCE is controlled by the mass transport of nitrite ions from the bulk solution to the electrode surface.

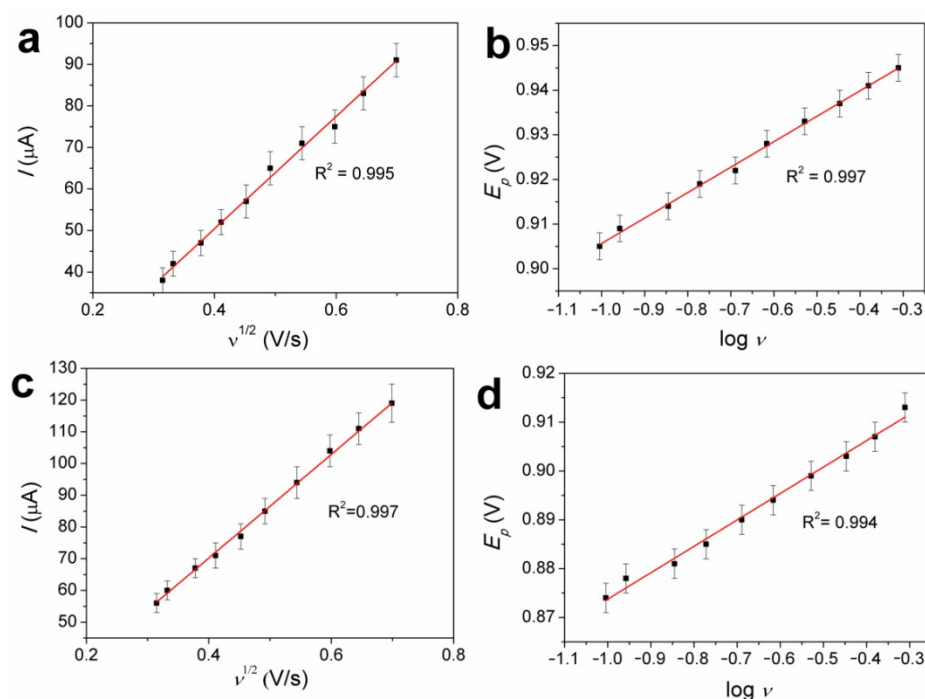


**Figure 5.**  $I$ - $\nu^{1/2}$  and  $E$ - $\log \nu$  dependences for the FePc(tBu)<sub>4</sub>/GCE (a,b) and Au/FePc(tBu)<sub>4</sub>/GCE (c,d).

**Table 2.**  $I$ - $\nu^{1/2}$  and  $E$ - $\log \nu$  dependences for the FePc(tBu)<sub>4</sub>/GCE and Au/FePc(tBu)<sub>4</sub>/GCE.

Electrode <sup>1</sup>	$I(\mu\text{A})-\nu^{1/2}(\text{V/s})^{1/2}$	$E(\text{V})-\log \nu$	$(1-\alpha)n\alpha$
FePc(tBu) <sub>4</sub> /GCE	$I = 6.781 + 167.4\nu^{1/2}$ ( $R^2 = 0.995$ )	$E = 1.343 + 0.058 \log \nu$ ( $R^2 = 0.997$ )	0.50
Au/FePc(tBu) <sub>4</sub> /GCE	$I = 7.833 + 163.9\nu^{1/2}$ ( $R^2 = 0.997$ )	$E = 1.554 + 0.054 \log \nu$ ( $R^2 = 0.994$ )	0.55
Au/FePc(tBu) <sub>4</sub> /GCE	$I = 8.033 + 190.9\nu^{1/2}$ ( $R^2 = 0.998$ )	$E = 0.954 + 0.089 \log \nu$ ( $R^2 = 0.997$ )	0.31

<sup>1</sup> Au/FePc(tBu)<sub>4</sub>/GCE was studied at potential range (−300–1200 mV).

To determine the number of electrons that participate in the rate-determining step ( $n\alpha$ ) and the electron transfer coefficient ( $\alpha$ ) values of the FePc(tBu)<sub>4</sub>/GCE and Au/FePc(tBu)<sub>4</sub>/GCE, the Laviron's expressions concerning the anodic peak potential of NO<sub>2</sub><sup>−</sup> ( $E_p$ ) vs. the logarithm scan rate ( $\log \nu$ ) were obtained (Figure 5b,d). The corresponding linear regression equations are listed in Table 2. Applying the Tafel equation (Equation (3)), the  $(1-\alpha)n\alpha$  values of the FePc(tBu)<sub>4</sub>/GCE and Au/FePc(tBu)<sub>4</sub>/GCE were calculated (Table 2, column 4)

$$E_p = (2.3RT/2[(1-\alpha)n\alpha]F)\log \nu + C, \quad (3)$$

where  $R$ ,  $T$ , and  $F$  values represent the universal gas constant, temperature, and Faraday's constant, respectively. From the estimated  $(1 - \alpha)n_\alpha$  values for the FePc(tBu)<sub>4</sub>/GCE and Au/FePc(tBu)<sub>4</sub>/GCE, the one-electron transfer in the rate-determining step (rds) was suggested. The Tafel values were calculated to be 116 and 108 mV/decade for the FePc(tBu)<sub>4</sub>/GCE and Au/FePc(tBu)<sub>4</sub>/GCE, respectively. According to the work of Partra et al. [61], a Tafel slope of less than 120 mV/dec indicates the high efficiency of an electron transfer and the low passivation of the electrode surface. The Au/FePc(tBu)<sub>4</sub>/GCE studied here demonstrates the best electron transfer characteristics; this is due to its increased surface area, which, in turn, is due to the AuNPs. It is important to note that we cannot completely exclude the possible role of the electrocatalytic oxidation of nitrites on Au cores in the range of potentials from  $-300$  to  $1000$  mV.

In addition, both  $I-v^{1/2}$  and  $E-\log v$  dependences for the Au/FePc(tBu)<sub>4</sub>/GCE (Figure S4) were plotted in the range of  $-300$ – $1200$  mV (Table 2). The Tafel slope for the Au/FePc(tBu)<sub>4</sub>/GCE increases from 108 to 188 mV/decade when the potential range changes. This means that the efficiency of electron transport on the Au/FePc(tBu)<sub>4</sub>/GCE, in the range of  $-300$ – $1200$  mV, decreases because of the passivation of the electrode surface due to subsequent chemical reactions involving gold ions shortly after electron transfer. In this case, it is possible to conclude that the electrocatalytic oxidation of NO<sub>2</sub><sup>−</sup> to NO<sub>2</sub> on Au<sup>0</sup> nanoparticles likely occurs via adsorption using the inner sphere mechanism [56,62].

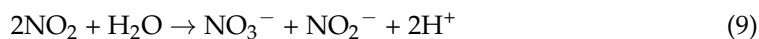
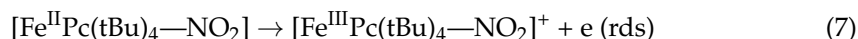
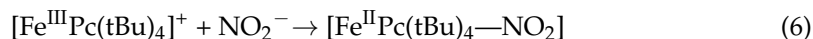
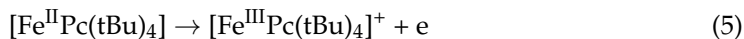
The AuNPs present in the modified electrodes form a [Au<sup>0</sup>–NO<sub>2</sub><sup>−</sup>] complex in the presence of nitrite. This complex is electrochemically oxidized to Au<sup>+</sup> and NO<sub>2</sub>, regardless of whether the reduction conversion of Au<sup>+</sup> to Au<sup>0</sup> is observed at the Au/FePc(tBu)<sub>4</sub> [56].

Finally, the total number of electrons ( $n$ ) transferred during the oxidation of nitrite ions on the surface of the FePc(tBu)<sub>4</sub>/GCE and Au/FePc(tBu)<sub>4</sub>/GCE ( $-300$ – $1000$  mV) is estimated from the  $I-v^{1/2}$  dependences (Table 2) using the Randles–Sevcik equation (Equation (4)), thus initiating an irreversible process:

$$I = 2.69 \times 10^5 [(1 - \alpha)n_\alpha]^{1/2} n A C D^{1/2} v^{1/2}, \quad (4)$$

where  $A$  and  $[(1 - \alpha)n_\alpha]$  are values from Tables 1 and 2,  $C$  (NO<sub>2</sub><sup>−</sup> concentration) is equal to  $0.25 \times 10^{-6}$  mol/cm<sup>3</sup>, and  $D$  is equal to  $2.1 \times 10^{-5}$  cm<sup>2</sup>/s [63]. From Equation (4), the  $n$  values are close to two for both the FePc(tBu)<sub>4</sub>/GCE and Au/FePc(tBu)<sub>4</sub>/GCE.

Thus, based on the analysis of the data in the literature [34,64], the following mechanism for nitrite oxidation on the FePc(tBu)<sub>4</sub>/GCE and Au/FePc(tBu)<sub>4</sub>/GCE was proposed. In the first stage, the Fe<sup>II</sup>Pc(tBu)<sub>4</sub> undergoes oxidation to Fe<sup>III</sup>Pc(tBu)<sub>4</sub> (Equation (5)), then, the formation of the adduct [Fe<sup>II</sup>Pc(tBu)<sub>4</sub>–NO<sub>2</sub>] takes place (see Equation (6)), whereas Equation (7) demonstrates the one-electron rate-determining step (rds). We believe that the deposition of AuNPs onto the FePc(tBu)<sub>4</sub>/GCE is accompanied by a decrease in the Tafel slope (due to an increase in the efficiency of the electron transfer to the Au/FePc(tBu)<sub>4</sub>/GCE compared with the electron transfer to the FePc(tBu)<sub>4</sub>/GCE). Equation (8) describes the regeneration of the initial [Fe<sup>II</sup>Pc(tBu)<sub>4</sub>] with the formation of NO<sub>2</sub>, which then undergoes a disproportionation reaction (see Equation (9)), thus resulting in the formation of NO<sub>2</sub><sup>−</sup> and NO<sub>3</sub><sup>−</sup> ions:



### 3.6. Nitrite Detection

Amperometric experiments with FePc(tBu)<sub>4</sub>/GCE and Au/FePc(tBu)<sub>4</sub>/GCE were carried out at 1 V under constant stirring conditions to induce a better interaction between the electrode and the electrolyte. Figure 6a shows a gradual increase in the oxidation current

on the  $I-t$  curves of both samples after each addition of  $2 \mu\text{M}$  of  $\text{NO}_2^-$ . As a result of the amperometric experiments on the  $\text{FePc}(\text{tBu})_4/\text{GCE}$  and  $\text{Au}/\text{FePc}(\text{tBu})_4/\text{GCE}$  electrodes, which were carried out in the  $\text{NO}_2^-$  concentration ranges of  $2\text{--}26 \mu\text{M}$  and  $20\text{--}120 \mu\text{M}$ , respectively, the calibration curves shown in Figure 6b,c were obtained.

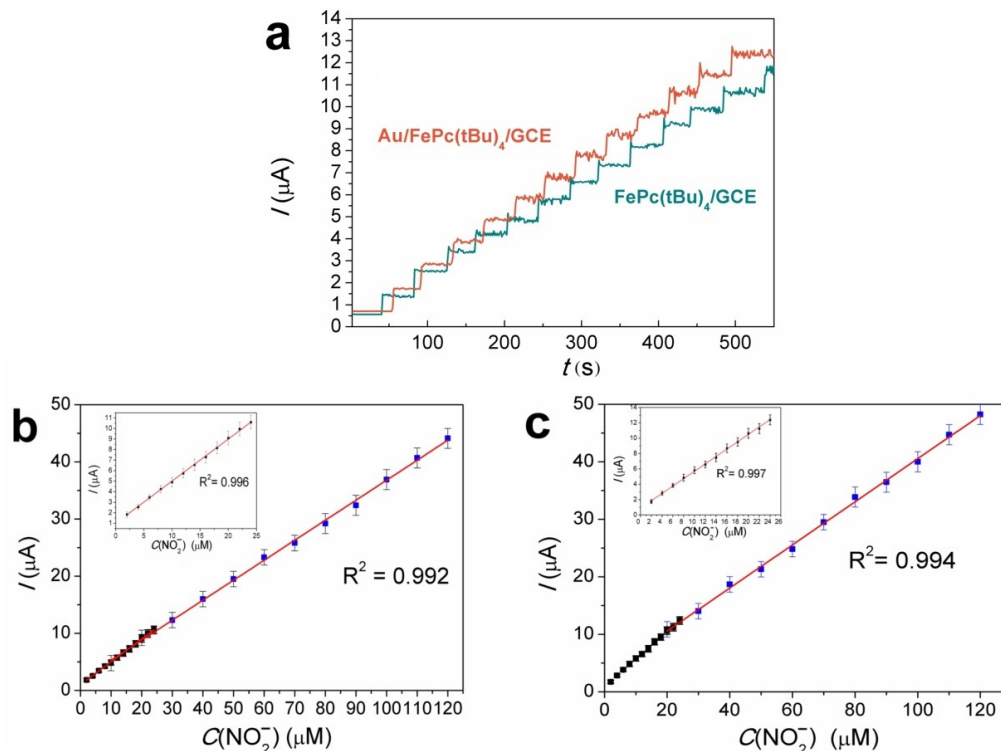


**Figure 6.** Amperometric response of the  $\text{FePc}(\text{tBu})_4/\text{GCE}$  and  $\text{Au}/\text{FePc}(\text{tBu})_4/\text{GCE}$  after the addition of nitrite ( $2\text{--}26 \mu\text{M}$ ) (a). Calibration plots of the peak current versus the  $\text{NO}_2^-$  concentration for the  $\text{FePc}(\text{tBu})_4/\text{GCE}$  (b) and  $\text{Au}/\text{FePc}(\text{tBu})_4/\text{GCE}$  (c).

Calibration curves demonstrate two different linear regions for both investigated electrodes. The curves in the concentration range from  $2$  to  $26 \mu\text{M}$  are described by the following equations:  $I(\mu\text{A}) = 0.675 + 0.362 C_{\text{NO}_2^-}$  ( $R^2 = 0.996$ ) and  $I(\mu\text{A}) = 0.87 + 0.455 C_{\text{NO}_2^-}$  ( $R^2 = 0.997$ ) for the  $\text{FePc}(\text{tBu})_4/\text{GCE}$  and  $\text{Au}/\text{FePc}(\text{tBu})_4/\text{GCE}$ , respectively. The calculated limits of detection (LOD) ( $S/N = 3$ ) were  $0.63$  and  $0.35 \mu\text{M}$  for the  $\text{FePc}(\text{tBu})_4/\text{GCE}$  and  $\text{Au}/\text{FePc}(\text{tBu})_4/\text{GCE}$ , respectively (Table 3). The sensitivities were  $0.36$  and  $0.46 \mu\text{A}\mu\text{M}^{-1}$  for the  $\text{FePc}(\text{tBu})_4/\text{GCE}$  and  $\text{Au}/\text{FePc}(\text{tBu})_4/\text{GCE}$ , respectively, whereas the sensitivity values per unit of the active surface of the electrode ( $A$ , Table 1) were  $0.8$  and  $0.87 \mu\text{A}\mu\text{M}^{-1} \text{cm}^{-2}$ .

The other linear regions, with slightly different slopes, are observed at  $\text{NO}_2^-$  concentrations ranging from  $20$  to  $120 \mu\text{M}$  (Figure 6b,c). These linear dependencies are described by the equations  $I(\mu\text{A}) = 1.79 + 0.334 C_{\text{NO}_2^-}$  ( $R^2 = 0.992$ ) and  $I(\mu\text{A}) = 3.65 + 0.419 C_{\text{NO}_2^-}$  ( $R^2 = 0.994$ ) for the  $\text{FePc}(\text{tBu})_4/\text{GCE}$  and  $\text{Au}/\text{FePc}(\text{tBu})_4/\text{GCE}$ , respectively (Figure 6b,c). A comparison of these dependencies indicates a  $5\text{--}6\%$  decrease in the sensitivity of both electrodes at higher concentrations of nitrite. This effect is probably associated with a decrease in electrochemically active centers due to the formation of a large amount of product on the electrode surface [65].

The results showed that the LOD of the  $\text{Au}/\text{FePc}(\text{tBu})_4/\text{GCE}$  is two times lower than that of the  $\text{FePc}(\text{tBu})_4/\text{GCE}$ . This is likely to be due to an increase in the surface area of the  $\text{Au}/\text{FePc}(\text{tBu})_4/\text{GCE}$ , due to the deposition of AuNPs. The analytical performance of the investigated sensors is compared with other nitrite sensors in Table 3. The literature analysis shows that the surface modification of GCE or graphene surfaces with AuNPs seems to be a good strategy for improving the characteristics of electrodes; this is due to the excellent conductivity of gold and the formation of active centers.

For example, the sensitivity of a GCE, modified with Au particles that are sized between 100–110 nm, obtained by electrodeposition, followed by 3-mercaptopropionic acid self-assembly, thus enabling attachment of an iron(III) monoamino-phthalocyanine via amide bond formation, was quite low [34]. On the other hand, composite materials with AuNPs particles demonstrated higher sensitivity values, which indicates the advantages of using composite materials for electrode modification due to their synergistic effects [56,65,66]. According to [7], the high sensitivity of the electrodes can be explained by the efficiency of the electron transfer between the modified electrode and nitrite. In our case, the modification of the FePc(tBu)<sub>4</sub>/GCE with small AuNPs has had a positive effect on electron transfer (see Section 3.4), and the Au/FePc(tBu)<sub>4</sub>/GCE exhibits a higher sensitivity compared with the FePc(tBu)<sub>4</sub>/GCE and some of the electrodes shown in Table 3.

**Table 3.** Comparison of the analytical performance of the FePc(tBu)<sub>4</sub>/GCE and Au/FePc(tBu)<sub>4</sub>/GCE with other nitrite sensors.

Electrode	Method (pH)	Concentration Range	LOD (μM)	Sensitivity (μAμM <sup>-1</sup> )	Ref.
AuNP/rGO HMS/GCE <sup>a</sup>	Amp (7)	0.5 μM–2.8 mM	0.5	-	[67]
Rose-like AuNPs/ MoS <sub>2</sub> nanoflower/graphene	Amp (4.7)	0.5 μM–5 mM	1	-	[68]
GCE modified with Pd/CoPc nanorods	DPV (6)	0–5 mM	0.1	0.01	[33]
Nano-Au/Ch/GCE <sup>b</sup>	DPV (7)	0.7–750 μM	0.1	0.35	[66]
Au-Fe(III) nanoparticle/GCE	DPV (7)	0.3–150 μM	0.3	0.13	[69]
FeMAPc-MPA/AuNPs/GCE	DPV (5.8)	1.9 μM–2 mM	0.21	0.015	[34]
AuNPs/GCE			-	0.008	
Dendrimer/AuNPs/GCE <sup>c</sup>	Amp (5)	10–5000 μM	0.2	-	[56]
CoTM-QOPc/CNP/GCE <sup>d</sup>	Amp (7)	0.1–350 μM	0.033	-	[21]
Fe(III)P/MWCNTs/GCE <sup>e</sup>	Amp (4)	1–600 μM 0.6–1.6 mM	0.5	-	[70]
FePc(tBu) <sub>4</sub> /GCE	Amp (6.8)	2–26 μM (20–120 μM)	0.63	0.36 (0.33)	This work
Au/FePc(tBu) <sub>4</sub> /GCE			0.35	0.46 (0.42)	

<sup>a</sup> HMS—hollow microspheres, CR-GO—chemically reduced graphene dioxide; <sup>b</sup> Ch—Choline; <sup>c</sup> Dendrimer/AuNPs—gold nanoparticles and a carbosilane-dendrimer possessing peripheral electronically communicated ferrocenyl units (Dend); <sup>d</sup> CoTM-QOPc/CNP—Cobalt (II) tetra methyl-quinoline oxy bridged phthalocyanine, CNT—carbon nanotubes, <sup>e</sup> Fe(III)P/MWCNTs—chloro [3,7,12,17-tetramethyl-8,13-divinylporphyrin-2,18-dipropanoato (2-)]iron(III)/multi-walled carbon nanotube composite.

In general, the characteristics of the sensors proposed in this work are comparable to the characteristics of sensors based on other materials, even surpassing some of them in terms of sensitivity. It should also be noted that in most of the works mentioned above, more complex methods and more expensive materials were used to modify the surface of the electrodes. With regard to our proposed sensors, all components are commercially available, and gas-phase deposition methods for both phthalocyanine films and gold nanoparticles make it possible to control the thickness of the layers and the ratio of components in the heterostructure. Moreover, it is also possible to obtain a large number of electrodes in one deposition cycle.

### 3.7. Selectivity, Stability, and Reproducibility of Au/FePc(tBu)<sub>4</sub>/GCE

The Au/FePc(tBu)<sub>4</sub>/GCE, which showed the best LOD and sensitivity in the studied series of samples, was examined in detail to assess its suitability for detecting nitrites in real samples of meat products. For this purpose, interfering analytes, viz. NaCl, NaNO<sub>3</sub>, glucose, sodium glutamate, and sodium ascorbate (Na(AA)), which can be found in real samples of meat products, were selected. Figure 7a shows no obvious change in the current

response after sequential injections of interfering ions (signal change less than 3%). Only in the case of  $AA^-$ , was a 5.5% signal change observed (from three parallel probes).

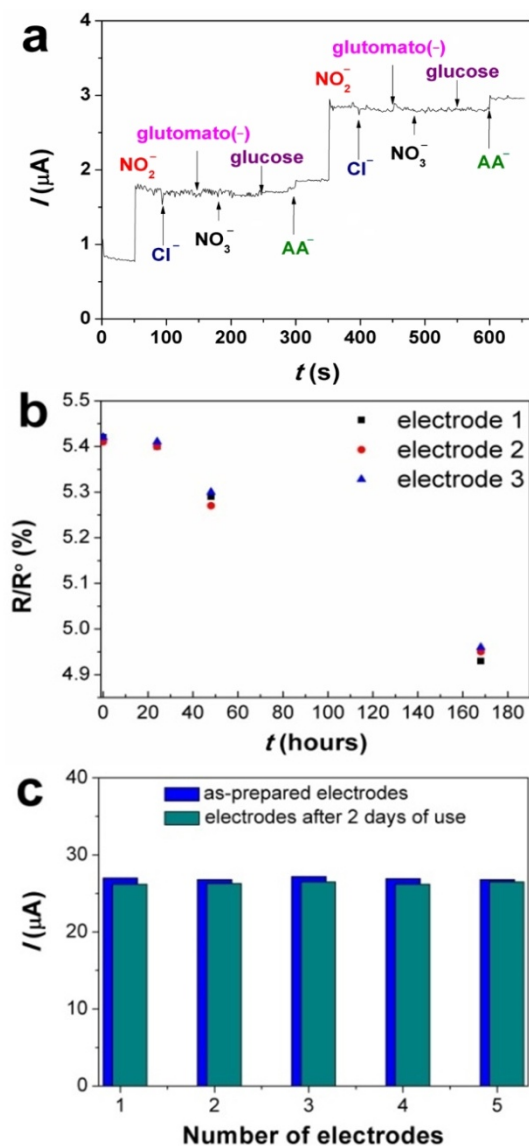


**Figure 7.** Amperometric response of the Au/FePc(tBu)<sub>4</sub>/GCE to various interfering analytes (a); stability of the amperometric response ( $R$ ) of the Au/FePc(tBu)<sub>4</sub>/GCE after the addition of  $10 \mu M NO_2^-$  (b); and the repeatability and reproducibility of the Au/FePc(tBu)<sub>4</sub>/GCE (c).

The stability response of the Au/FePc(tBu)<sub>4</sub>/GCE to  $NO_2^-$  was studied in 0.1 M PBS in the presence of  $10 \mu M NaNO_2$  at a working potential of 1 V. The obtained amperometric current responses of three Au/FePc(tBu)<sub>4</sub>/GCE samples are plotted in Figure 7b. The stability of the Au/FePc(tBu)<sub>4</sub>/GCE response to  $NO_2^-$  was studied in 0.1 M PBS in the presence of  $10 \mu M NaNO_2$  at a working potential of 1 V. The obtained amperometric current responses of three Au/FePc(tBu)<sub>4</sub>/GCE samples are shown in Figure 7b. After one day, the sensor response changed by no more than 1%, whereas after two and seven days, it decreased by no more than 2.4 and 5.1%, respectively. Thus, the measured response of the Au/FePc(tBu)<sub>4</sub>/GCE to  $NO_2^-$  oxidation shows good stability.

To determine the reproducibility of both, in terms of preparation and reusability, the Au/FePc(tBu)<sub>4</sub>/GCE was evaluated for a series of five identical samples. CV measurements were carried out in 0.1 M PBS with 0.1 mM of  $NO_2^-$  under identical experimental conditions ( $-300-1000$  mV,  $v = 100$  mV/s) (Figure 7c). The relative standard deviation (RSD) values

for the anodic peak current were measured using a series of five electrodes. Before and after their operation, the values were estimated to be 1.9% and 2.7%, respectively, which indicates a good reproducibility with regard to the  $\text{NO}_2^-$  response.

### 3.8. Real Meat Food Sample Analysis Using Au/FePc(tBu)<sub>4</sub>/GCE

The practical applicability of the Au/FePc(tBu)<sub>4</sub>/GCE was verified by determining the presence of  $\text{NO}_2^-$  in two samples of meat products. In the first stage, preliminary measurements of the concentration of nitrites in both food samples were carried out. Based on these data, the calibration curve  $I(\mu\text{A}) = 0.87 + 0.455 C_{\text{NO}_2^-}$  ( $R^2 = 0.994$ ) which contained a range of nitrite concentrations, from 2 to 26  $\mu\text{M}$ , was selected. Then, the standard addition method was used to verify the accuracy of the proposed calibration (Table 4, columns 2, 3).

**Table 4.** Determination of nitrite in Sample 1 (smoked sausages) and Sample 2 (sausages) using the Au/FePc(tBu)<sub>4</sub>/GCE ( $n = 5$ ).

Food Sample	Added ( $\mu\text{M}$ )	Found ( $\mu\text{M}$ )	Recovery (%)	Nitrite in Sample mg/kg
Sample 1	3.00	$2.91 \pm 0.18$	97	$15.56 \pm 0.63$
	5.00	$5.12 \pm 0.27$	102	
	9.00	$9.29 \pm 0.34$	103	
Sample 2	3.00	$3.15 \pm 0.21$	105	$11.38 \pm 0.48$
	5.00	$4.90 \pm 0.29$	98	
	9.00	$9.24 \pm 0.37$	103	

The recovery percentages of nitrite detected in the samples ranged from 97 to 105% (Table 4, column 4), whereas the RSD values did not exceed 7% (Table 4, column 3). The satisfactory recovery and RSD values indicate that the Au/FePc(tBu)<sub>4</sub>/GCE sensor is suitable for detecting nitrites in real samples.

Finally, using this calibration curve, the concentrations of nitrite in both samples were determined and then attributed to the mass of the meat product (5 g, see Section 2.4). The content of nitrites in smoked sausages and sausages (Table 4, column 5) was determined to be  $15.56 \pm 0.63$  and  $11.38 \pm 0.48$  mg/kg, respectively.

A comparison of the nitrite content in the studied samples, with the data published in some reports [7,71,72], showed an adequate concentration of nitrite in both food samples. It should also be noted that the amount of nitrite found in the examined samples of meat products did not exceed the standards recommended by the European Food Safety Authority (EFSA) [73].

## 4. Conclusions

Electrochemical sensors based on a glass carbon electrode (GCE), modified with Fe(II) tetra-tert-butyl phthalocyanine film (FePc(tBu)<sub>4</sub>/GCE) and a heterostructure with gold nanoparticles (Au/FePc(tBu)<sub>4</sub>/GCE), were obtained using a facile gas-phase deposition technique. Their composition and morphology were examined using spectroscopy and microscopy methods. The Au/FePc(tBu)<sub>4</sub>/GCE, with uniformly distributed 9–11 nm AuNPs, exhibited a high surface-to-volume ratio, and its active surface area reached 0.523 nm. All components of the proposed sensors are comparatively cheap and commercially available, and they were deposited on the surface of the GCE via a physical vapor deposition technique; this makes it possible to control the ratio of components in the heterostructure and to obtain a large number of electrodes in one deposition cycle.

The optimal conditions for cyclic voltammetry (CV) experiments involving nitrite oxidation on the FePc(tBu)<sub>4</sub>/GCE and Au/FePc(tBu)<sub>4</sub>/GCE were determined to be as follows. The electrodes should be placed in 0.1 M phosphate buffer (pH = 6.8), in the potential ranges of  $-300$ – $1200$  mV and  $-300$ – $1000$  mV, respectively. The CV results showed that the Au/FePc(tBu)<sub>4</sub>/GCE had the highest efficiency in terms of nitrite oxidation, due to its enhanced current response and the fact that it had the lowest oxidation potential compared

with the bare GCE and FePc(tBu)<sub>4</sub>/GCE; this illustrates the potential of combining metal phthalocyanines with gold nanoparticles.

The sensor based on the Au/FePc(tBu)<sub>4</sub>/GCE had a low limit of detection at 0.35 μM, along with a high sensitivity to nitrite ions of 0.46 μA μM<sup>-1</sup>. The proposed Au/FePc(tBu)<sub>4</sub>/GCE demonstrated good repeatability and reproducibility, as well as long-term response stability. The interference study showed that it exhibited a selective response to NO<sub>2</sub><sup>-</sup> in the presence of interfering anions, indicating that the proposed Au/FePc(tBu)<sub>4</sub> heterostructure would be a promising material for the production of sensors that determine nitrite ions in food.

**Supplementary Materials:** The following supporting information can be downloaded at: <https://www.mdpi.com/article/10.3390/s22155780/s1>, Figure S1: CV curves of Au/FePc(tBu)<sub>4</sub>/GCE, recorded at (−300–1200 mV); Figure S2: EDX spectrum of Au/FePc(tBu)<sub>4</sub>/GCE; Figure S3: N 1s spectra of FePc(tBu)<sub>4</sub>/GCE (a) and O 1s spectra of FePc(tBu)<sub>4</sub>/GCE (b); Figure S4:  $I-v^{1/2}$  (a) and  $E-\log v$  (b) dependences for Au/FePc(tBu)<sub>4</sub>/GCE, recorded in the presence of 0.25 mM nitrite at (−300–1200 mV).

**Author Contributions:** Conceptualization, S.I.D. and T.V.B.; methodology, S.I.D. and T.V.B.; validation, S.I.D. and D.D.K.; formal analysis, S.I.D. and T.V.B.; investigation, S.I.D., A.D.F. and D.D.K.; resources, S.I.D.; data curation, S.I.D. and D.D.K.; writing—original draft preparation, S.I.D. and T.V.B.; writing—review and editing, S.I.D., D.D.K., N.B.M. and T.V.B.; visualization, S.I.D.; supervision, T.V.B. and N.B.M.; project administration, S.I.D.; funding acquisition, S.I.D. and T.V.B. All authors have read and agreed to the published version of the manuscript.

**Funding:** The part of this study that is devoted to the characterization of the FePc(tBu)<sub>4</sub>/GCE and Au/FePc(tBu)<sub>4</sub>/GCE, and the investigation of their sensor response to nitrites in water solutions, was funded by the Russian Science Foundation (grant 21-73-10142). The part of this study that is devoted to the investigation of the sensor response to nitrites in meat products was funded by the Russian Ministry of Education and Science (project 121031700314-5).

**Institutional Review Board Statement:** Not applicable.

**Informed Consent Statement:** Not applicable.

**Data Availability Statement:** Not applicable.

**Acknowledgments:** The authors acknowledge the Russian Ministry of Education and Science for the access to literature search databases.

**Conflicts of Interest:** The authors declare no conflict of interest.

## References

1. Neth, M.R.; Love, J.S.; Horowitz, B.Z.; Shertz, M.D.; Sahni, R.; Daya, M.R. Fatal Sodium Nitrite Poisoning: Key Considerations for Prehospital Providers. *Prehospital Emerg. Care* **2021**, *25*, 844–850. [[CrossRef](#)]
2. Tricker, A.R.; Preussmann, R. Carcinogenic N-nitrosamines in the diet: Occurrence, formation, mechanisms and carcinogenic potential. *Mutat. Res. Toxicol.* **1991**, *259*, 277–289. [[CrossRef](#)]
3. Sudarvizhi, A.; Siddiqha, Z.A.; Pandian, K. Single step synthesis of graphene oxide protected silver nanoparticles using aniline as reducing agent and study its application on electrocatalytic detection of nitrite in food samples. *J. Chem. Appl. Biochem.* **2014**, *1*, 101.
4. Abdulmumeen, H.A.; Risikat, A.N.; Sururah, A.R. Food: Its preservatives, additives and applications. *Int. J. Chem. Biochem. Sci.* **2012**, *1*, 36–47. [[CrossRef](#)]
5. Martinez, J.; Dabert, P.; Barrington, S.; Burton, C. Livestock waste treatment systems for environmental quality, food safety, and sustainability. *Bioresour. Technol.* **2009**, *100*, 5527–5536. [[CrossRef](#)]
6. Coviello, D.; Pascale, R.; Ciriello, R.; Salvi, A.M.; Guerrieri, A.; Contursi, M.; Scrano, L.; Bufo, S.A.; Cataldi, T.R.I.; Bianco, G. Validation of an analytical method for nitrite and nitrate determination in meat foods for infants by ion chromatography with conductivity detection. *Foods* **2020**, *9*, 1238. [[CrossRef](#)] [[PubMed](#)]
7. Santos, W.J.R.; Lima, P.R.; Tanaka, A.A.; Tanaka, S.M.C.N.; Kubota, L.T. Determination of nitrite in food samples by anodic voltammetry using a modified electrode. *Food Chem.* **2009**, *113*, 1206–1211. [[CrossRef](#)]
8. Da Silva, S.; Cosnier, S.; Almeida, M.G.; Moura, J.J.G. An efficient poly(pyrrole-viologen)-nitrite reductase biosensor for the mediated detection of nitrite. *Electrochem. Commun.* **2004**, *6*, 404–408. [[CrossRef](#)]
9. Da Rocha, J.; Angnes, L.; Bertotti, M.; Araki, K.; Toma, H. Amperometric detection of nitrite and nitrate at tetra-ruthenated porphyrin-modified electrodes in a continuous-flow assembly. *Anal. Chim. Acta* **2002**, *452*, 23–28. [[CrossRef](#)]

10. Chen, L.; Liu, X.; Wang, C.; Lv, S.; Chen, C. Amperometric nitrite sensor based on a glassy carbon electrode modified with electrodeposited poly(3,4-ethylenedioxythiophene) doped with a polyacenic semiconductor. *Microchim. Acta* **2017**, *184*, 2073–2079. [[CrossRef](#)]
11. Zhang, Y.; Chen, P.; Wen, F.; Huang, C.; Wang, H. Construction of polyaniline/molybdenum sulfide nanocomposite: Characterization and its electrocatalytic performance on nitrite. *Ionics* **2016**, *22*, 1095–1102. [[CrossRef](#)]
12. Wang, G.; Han, R.; Feng, X.; Li, Y.; Lin, J.; Luo, X. A glassy carbon electrode modified with poly(3,4-ethylenedioxythiophene) doped with nano-sized hydroxyapatite for amperometric determination of nitrite. *Microchim. Acta* **2017**, *184*, 1721–1727. [[CrossRef](#)]
13. Fan, X.; Lin, P.; Liang, S.; Hui, N.; Zhang, R.; Feng, J.; Xu, G. Gold nanoclusters doped poly(3,4-ethylenedioxythiophene) for highly sensitive electrochemical sensing of nitrite. *Ionics* **2017**, *23*, 997–1003. [[CrossRef](#)]
14. Deng, K.; Zhou, J.; Huang, H.; Ling, Y.; Li, C. Electrochemical Determination of Nitrite Using a Reduced Graphene Oxide–Multiwalled Carbon Nanotube-Modified Glassy Carbon Electrode. *Anal. Lett.* **2016**, *49*, 2917–2930. [[CrossRef](#)]
15. Rabti, A.; Ben Aoun, S.; Raouafi, N. A sensitive nitrite sensor using an electrode consisting of reduced graphene oxide functionalized with ferrocene. *Microchim. Acta* **2016**, *183*, 3111–3117. [[CrossRef](#)]
16. Sheng, Q.; Liu, D.; Zheng, J. A nonenzymatic electrochemical nitrite sensor based on Pt nanoparticles loaded Ni(OH)<sub>2</sub>/multiwalled carbon nanotubes nanocomposites. *J. Electroanal. Chem.* **2017**, *796*, 9–16. [[CrossRef](#)]
17. Cui, L.; Zhu, J.; Meng, X.; Yin, H.; Pan, X.; Ai, S. Controlled chitosan coated Prussian blue nanoparticles with the mixture of graphene nanosheets and carbon nanospheres as a redox mediator for the electrochemical oxidation of nitrite. *Sens. Actuators B Chem.* **2012**, *161*, 641–647. [[CrossRef](#)]
18. Sudarvizhi, A.; Pandian, K.; Oluwafemi, O.S.; Gopinath, S.C.B. Amperometry detection of nitrite in food samples using tetrasulfonated copper phthalocyanine modified glassy carbon electrode. *Sens. Actuators B Chem.* **2018**, *272*, 151–159. [[CrossRef](#)]
19. Matemadombo, F.; Nyokong, T. Characterization of self-assembled monolayers of iron and cobalt octaalkylthiosubstituted phthalocyanines and their use in nitrite electrocatalytic oxidation. *Electrochim. Acta* **2007**, *52*, 6856–6864. [[CrossRef](#)]
20. Aralekallu, S.; Mohammed, I.; Manjunatha, N.; Palanna, M.; Dhanjai; Sannegowda, L.K. Synthesis of novel azo group substituted polymeric phthalocyanine for amperometric sensing of nitrite. *Sens. Actuators B Chem.* **2019**, *282*, 417–425. [[CrossRef](#)]
21. Jilani, B.S.; Mounesh; Malathesh, P.; Mruthyunjayachari, C.D.; Reddy, K.R.V. Cobalt (II) tetra methyl-quinoline oxy bridged phthalocyanine carbon nano particles modified glassy carbon electrode for sensing nitrite: A voltammetric study. *Mater. Chem. Phys.* **2020**, *239*, 121920. [[CrossRef](#)]
22. Lu, S.; Jia, H.; Hummel, M.; Wu, Y.; Wang, K.; Qi, X.; Gu, Z. Two-dimensional conductive phthalocyanine-based metal-organic frameworks for electrochemical nitrite sensing. *RSC Adv.* **2021**, *11*, 4472–4477. [[CrossRef](#)] [[PubMed](#)]
23. Baranton, S.; Coutanceau, C.; Garnier, E.; Léger, J.M. How does  $\alpha$ -FePc catalysts dispersed onto high specific surface carbon support work towards oxygen reduction reaction (orr)? *J. Electroanal. Chem.* **2006**, *590*, 100–110. [[CrossRef](#)]
24. Mamuru, S.A.; Ozoemena, K.I. Impedimetric and electrocatalytic properties of nanostructured iron(II) phthalocyanine at pyrolytic graphite electrode. *Mater. Chem. Phys.* **2009**, *114*, 113–119. [[CrossRef](#)]
25. Zagal, J.H.; Griveau, S.; Silva, J.F.; Nyokong, T.; Bedioui, F. Metallophthalocyanine-based molecular materials as catalysts for electrochemical reactions. *Coord. Chem. Rev.* **2010**, *254*, 2755–2791. [[CrossRef](#)]
26. Sousa, A.L.; Santos, W.J.R.; Luz, R.C.S.; Damos, F.S.; Kubota, L.T.; Tanaka, A.A.; Tanaka, S.M.C.N. Amperometric sensor for nitrite based on copper tetrasulfonated phthalocyanine immobilized with poly-L-lysine film. *Talanta* **2008**, *75*, 333–338. [[CrossRef](#)]
27. Maringa, A.; Antunes, E.; Nyokong, T. Electrochemical behaviour of gold nanoparticles and Co tetraaminophthalocyanine on glassy carbon electrode. *Electrochim. Acta* **2014**, *121*, 93–101. [[CrossRef](#)]
28. Wang, Y.; Qu, J.; Wu, R.; Lei, P. The electrocatalytic reduction of nitrate in water on Pd/Sn-modified activated carbon fiber electrode. *Water Res.* **2006**, *40*, 1224–1232. [[CrossRef](#)]
29. Wu, Y.Y.; Li, C.; Dou, Z.Y.; Cui, L.L.; Liu, D.J.; He, X.Q. A novel nitrite sensor fabricated through anchoring nickel-tetrahydroxyphthalocyanine and polyethylene oxide film onto glassy carbon electrode by a two-step covalent modification approach. *J. Solid State Electrochem.* **2014**, *18*, 2625–2635. [[CrossRef](#)]
30. Lee, Y.-L.; Hsiao, C.-Y.; Chang, C.-H.; Yang, Y.-M. Effects of sensing temperature on the gas sensing properties of copper phthalocyanine and copper tetra-tert-butyl phthalocyanine films. *Sens. Actuators B Chem.* **2003**, *94*, 169–175. [[CrossRef](#)]
31. Klyamer, D.; Bonegardt, D.; Krasnov, P.; Sukhikh, A.; Popovetskiy, P.; Khezami, K.; Durmuş, M.; Basova, T. Halogen-substituted zinc(II) phthalocyanines: Spectral properties and structure of thin films. *Thin Solid Films* **2022**, *754*, 139301. [[CrossRef](#)]
32. Basova, T.V.; Ray, A.K. Review—Hybrid Materials Based on Phthalocyanines and Metal Nanoparticles for Chemiresistive and Electrochemical Sensors: A Mini-Review. *ECS J. Solid State Sci. Technol.* **2020**, *9*, 061001. [[CrossRef](#)]
33. Song, X.; Gao, L.; Li, Y.; Mao, L.; Yang, J.H. A sensitive and selective electrochemical nitrite sensor based on a glassy carbon electrode modified with cobalt phthalocyanine-supported Pd nanoparticles. *Anal. Methods* **2017**, *9*, 3166–3171. [[CrossRef](#)]
34. Saeed, A.A.; Singh, B.; Abbas, M.N.; Issa, Y.M.; Dempsey, E. Electrocatalytic Nitrite Determination Using Iron Phthalocyanine Modified Gold Nanoparticles. *Electroanalysis* **2015**, *27*, 1086–1096. [[CrossRef](#)]
35. Shumba, M.; Nyokong, T. Characterization and Electrocatalytic Activity of Nanocomposites Consisting of Nanosized Cobalt Tetraaminophenoxy Phthalocyanine, Multi-walled Carbon Nanotubes and Gold Nanoparticles. *Electroanalysis* **2016**, *28*, 1478–1488. [[CrossRef](#)]
36. Maringa, A.; Nyokong, T. The influence of gold nanoparticles on the electroactivity of nickel tetrasulfonated phthalocyanine. *J. Porphy. Phthalocyanines* **2014**, *18*, 642–651. [[CrossRef](#)]

37. Arlyapov, V.A.; Kharkova, A.S.; Kurbanaliyeva, S.K.; Kuznetsova, L.S.; Machulin, A.V.; Tarasov, S.E.; Melnikov, P.V.; Ponamoreva, O.N.; Alferov, V.A.; Reshetilov, A.N. Use of biocompatible redox-active polymers based on carbon nanotubes and modified organic matrices for development of a highly sensitive BOD biosensor. *Enzym. Microb. Technol.* **2021**, *143*, 109706. [[CrossRef](#)]
38. N'Diaye, J.; Bagchi, R.; Howe, J.Y.; Lian, K. Redox Active Organic-Carbon Composites for Capacitive Electrodes: A Review. *Sustain. Chem.* **2021**, *2*, 407–440. [[CrossRef](#)]
39. Fang, D.; Gao, G.; Yang, Y.; Wang, Y.; Gao, L.; Zhi, J. Redox Mediator-Based Microbial Biosensors for Acute Water Toxicity Assessment: A Critical Review. *ChemElectroChem* **2020**, *7*, 2513–2526. [[CrossRef](#)]
40. Kim, K.; Park, J.; Kim, H.; Jung, G.Y.; Kim, M.-G. Solid-Phase Photocatalysts: Physical Vapor Deposition of Au Nanoislands on Porous TiO<sub>2</sub> Films for Millimolar H<sub>2</sub>O<sub>2</sub> Production within a Few Minutes. *ACS Catal.* **2019**, *9*, 9206–9211. [[CrossRef](#)]
41. Wang, Y.; Limon-Petersen, J.G.; Compton, R.G. Measurement of the diffusion coefficients of [Ru(NH<sub>3</sub>)<sub>6</sub>]<sup>3+</sup> and [Ru(NH<sub>3</sub>)<sub>6</sub>]<sup>2+</sup> in aqueous solution using microelectrode double potential step chronoamperometry. *J. Electroanal. Chem.* **2011**, *652*, 13–17. [[CrossRef](#)]
42. Sallan, S.; Kaban, G.; Kaya, M. The effects of nitrite, sodium ascorbate and starter culture on volatile compounds of a semi-dry fermented sausage. *LWT* **2022**, *153*, 112540. [[CrossRef](#)]
43. Ramezani, H.; Abhari, K.; Pilevar, Z.; Hosseini, H.; Mohammadi, A. Volatile N-nitrosamine, residual nitrite, and ascorbic acid levels in sausages during storage. *Foods Raw Mater.* **2020**, *8*, 107–114. [[CrossRef](#)]
44. Oyarzún, M.P.; Silva, N.; Cortés-Arriagada, D.; Silva, J.F.; Ponce, I.O.; Flores, M.; Tammeveski, K.; Bélanger, D.; Zitolo, A.; Jaouen, F.; et al. Enhancing the electrocatalytic activity of Fe phthalocyanines for the oxygen reduction reaction by the presence of axial ligands: Pyridine-functionalized single-walled carbon nanotubes. *Electrochim. Acta* **2021**, *398*, 139263. [[CrossRef](#)]
45. Venegas, R.; Recio, F.J.; Zuñiga, C.; Viera, M.; Oyarzún, M.P.; Silva, N.; Neira, K.; Marco, J.F.; Zagal, J.H.; Tasca, F. Comparison of the catalytic activity for O<sub>2</sub> reduction of Fe and Co MN4 adsorbed on graphite electrodes and on carbon nanotubes. *Phys. Chem. Chem. Phys.* **2017**, *19*, 20441–20450. [[CrossRef](#)] [[PubMed](#)]
46. Ottaviano, L.; Lozzi, L.; Ramondo, F.; Picozzi, P.; Santucci, S. Copper hexadecafluoro phthalocyanine and naphthalocyanine: The role of shake up excitations in the interpretation and electronic distinction of high-resolution X-ray photoelectron spectroscopy measurements. *J. Electron Spectrosc. Relat. Phenom.* **1999**, *105*, 145–154. [[CrossRef](#)]
47. Åhlund, J.; Nilson, K.; Schiessling, J.; Kjeldgaard, L.; Berner, S.; Mårtensson, N.; Puglia, C.; Brena, B.; Nyberg, M.; Luo, Y. The electronic structure of iron phthalocyanine probed by photoelectron and x-ray absorption spectroscopies and density functional theory calculations. *J. Chem. Phys.* **2006**, *125*, 034709. [[CrossRef](#)] [[PubMed](#)]
48. Evangelista, F.; Ruocco, A.; Gotter, R.; Cossaro, A.; Floreano, L.; Morgante, A.; Crispoldi, F.; Betti, M.G.; Mariani, C. Electronic states of CuPc chains on the Au(110) surface. *J. Chem. Phys.* **2009**, *131*, 174710. [[CrossRef](#)]
49. Alfredsson, Y.; Brena, B.; Nilson, K.; Åhlund, J.; Kjeldgaard, L.; Nyberg, M.; Luo, Y.; Mårtensson, N.; Sandell, A.; Puglia, C.; et al. Electronic structure of a vapor-deposited metal-free phthalocyanine thin film. *J. Chem. Phys.* **2005**, *122*, 214723. [[CrossRef](#)]
50. Suresh Kumar, P.; Lakshminarayanan, V. Electron-Transfer Studies in a Lyotropic Columnar Hexagonal Liquid Crystalline Medium. *Langmuir* **2006**, *23*, 1548–1554. [[CrossRef](#)] [[PubMed](#)]
51. Holm, T.; Ingdál, M.; Fanavoll, E.V.; Sunde, S.; Seland, F.; Harrington, D.A. Mass-transport impedance at channel electrodes: Accurate and approximate solutions. *Electrochim. Acta* **2016**, *202*, 84–89. [[CrossRef](#)]
52. Ji, X.; Banks, C.E.; Crossley, A.; Compton, R.G. Oxygenated edge plane sites slow the electron transfer of the ferro-/ferricyanide redox couple at graphite electrodes. *ChemPhysChem* **2006**, *7*, 1337–1344. [[CrossRef](#)] [[PubMed](#)]
53. Schrattenecker, J.D.; Heer, R.; Melnik, E.; Maier, T.; Fafilek, G.; Hainberger, R. Hexaammineruthenium (II)/(III) as alternative redox-probe to Hexacyanoferrat (II)/(III) for stable impedimetric biosensing with gold electrodes. *Biosens. Bioelectron.* **2019**, *127*, 25–30. [[CrossRef](#)] [[PubMed](#)]
54. Miao, P.; Liang, Z.; Liu, L.; Chen, G. Fabrication of Multi-functionalized Gold Nanoparticles and the Application to Electrochemical Detection of Nitrite. *Curr. Nanosci.* **2011**, *7*, 354–358. [[CrossRef](#)]
55. Gutierrez, A.P.; Griveau, S.; Richard, C.; Pailleret, A.; Granados, S.G.; Bediouia, F. Hybrid materials from carbon nanotubes, nickel tetrasulfonated phthalocyanine and thin polymer layers for the selective electrochemical activation of nitric oxide in solution. *Electroanalysis* **2009**, *21*, 2303–2310. [[CrossRef](#)]
56. Losada, J.; García Armada, M.P.; García, E.; Casado, C.M.; Alonso, B. Electrochemical preparation of gold nanoparticles on ferrocenyl-dendrimer film modified electrodes and their application for the electrocatalytic oxidation and amperometric detection of nitrite. *J. Electroanal. Chem.* **2017**, *788*, 14–22. [[CrossRef](#)]
57. Ozoemena, K.; Nyokong, T. Voltammetric characterization of the self-assembled monolayer (SAM) of octabutylthiophthalocyaninatoiron(II): A potential electrochemical sensor. *Electrochim. Acta* **2002**, *47*, 4035–4043. [[CrossRef](#)]
58. Lu, S.; Yang, C.; Nie, M. Hydrothermal synthesized urchin-like nickel-cobalt carbonate hollow spheres for sensitive amperometric detection of nitrite. *J. Alloys Compd.* **2017**, *708*, 780–786. [[CrossRef](#)]
59. Lu, S.; Hummel, M.; Kang, S.; Gu, Z. Selective Voltammetric Determination of Nitrite Using Cobalt Phthalocyanine Modified on Multiwalled Carbon Nanotubes. *J. Electrochem. Soc.* **2020**, *167*, 046515. [[CrossRef](#)]
60. Cui, Y.; Yang, C.; Zeng, W.; Oyama, M.; Pu, W.; Zhang, J. Electrochemical Determination of Nitrite Using a Gold Nanoparticles-modified Glassy Carbon Electrode Prepared by the Seed-mediated Growth Technique. *Anal. Sci.* **2007**, *23*, 1421–1425. [[CrossRef](#)]
61. Patra, S.; Munichandraiah, N. Electrochemical reduction of hydrogen peroxide on stainless steel. *J. Chem. Sci.* **2009**, *121*, 675–683. [[CrossRef](#)]

62. Piela, B.; Wrona, P.K. Oxidation of Hydroxylamine on the Rotating Solid Electrodes. *J. Electrochem. Soc.* **2004**, *151*, E69–E79. [[CrossRef](#)]
63. Santos, W.J.R.; Sousa, A.L.; Luz, R.C.S.; Damos, F.S.; Kubota, L.T.; Tanaka, A.A.; Tanaka, S.M.C.N. Amperometric sensor for nitrite using a glassy carbon electrode modified with alternating layers of iron(III) tetra-(N-methyl-4-pyridyl)-porphyrin and cobalt(II) tetrasulfonated phthalocyanine. *Talanta* **2006**, *70*, 588–594. [[CrossRef](#)]
64. Wang, Y.; Ward, K.R.; Laborda, E.; Salter, C.; Crossley, A.; Jacobs, R.M.J.; Compton, R.G. A joint experimental and computational search for authentic nano-electrocatalytic effects: Electrooxidation of nitrite and L-ascorbate on gold nanoparticle-modified glassy carbon electrodes. *Small* **2013**, *9*, 478–486. [[CrossRef](#)] [[PubMed](#)]
65. Manikandan, V.S.; Durairaj, S.; Boateng, E.; Sidhureddy, B.; Chen, A. Electrochemical Detection of Nitrite Based on Co<sub>3</sub>O<sub>4</sub>-Au Nanocomposites for Food Quality Control. *J. Electrochem. Soc.* **2021**, *168*, 107505. [[CrossRef](#)]
66. Wang, P.; Mai, Z.; Dai, Z.; Li, Y.; Zou, X. Construction of Au nanoparticles on choline chloride modified glassy carbon electrode for sensitive detection of nitrite. *Biosens. Bioelectron.* **2009**, *24*, 3242–3247. [[CrossRef](#)] [[PubMed](#)]
67. Zhang, F.; Yuan, Y.; Zheng, Y.; Wang, H.; Liu, T.; Hou, S. A glassy carbon electrode modified with gold nanoparticle-encapsulated graphene oxide hollow microspheres for voltammetric sensing of nitrite. *Microchim. Acta* **2017**, *184*, 1565–1572. [[CrossRef](#)]
68. Han, Y.; Zhang, R.; Dong, C.; Cheng, F.; Guo, Y. Sensitive electrochemical sensor for nitrite ions based on rose-like AuNPs/MoS<sub>2</sub>/graphene composite. *Biosens. Bioelectron.* **2019**, *142*, 111529. [[CrossRef](#)]
69. Liu, T.S.; Kang, T.F.; Lu, L.P.; Zhang, Y.; Cheng, S.Y. Au-Fe(III) nanoparticle modified glassy carbon electrode for electrochemical nitrite sensor. *J. Electroanal. Chem.* **2009**, *632*, 197–200. [[CrossRef](#)]
70. Wang, C.; Yuan, R.; Chai, Y.; Chen, S.; Zhang, Y.; Hu, F.; Zhang, M. Non-covalent iron(III)-porphyrin functionalized multi-walled carbon nanotubes for the simultaneous determination of ascorbic acid, dopamine, uric acid and nitrite. *Electrochim. Acta* **2012**, *62*, 109–115. [[CrossRef](#)]
71. Thomas, D.; Rajith, L.; Lonappan, L.; Issac, S.; Kumar, K.G. Sensitive determination of nitrite in food samples using voltammetric techniques. *Food Anal. Methods* **2012**, *5*, 752–758. [[CrossRef](#)]
72. Yang, C.; Lu, Q.; Hu, S. A novel nitrite amperometric sensor and its application in food analysis. *Electroanalysis* **2006**, *18*, 2188–2193. [[CrossRef](#)]
73. Merino, L.; Örnemark, U.; Toldrá, F. Analysis of Nitrite and Nitrate in Foods: Overview of Chemical, Regulatory and Analytical Aspects. *Adv. Food Nutr. Res.* **2017**, *81*, 65–107. [[CrossRef](#)] [[PubMed](#)]